IJMMM International Journal of Minerals, Metallurgy and Materials 矿物冶金与材料学报（英文版）

Ultrahigh cycle fatigue fracture mechanism of high-quality bearing steel obtained through different deoxidation methods

Wei Xiao, Yan-ping Bao, Chao Gu, Min Wang, Yu Liu, Yong-sheng Huang, and Guang-tao Sun

Cite this article as:

Wei Xiao, Yan-ping Bao, Chao Gu, Min Wang, Yu Liu, Yong-sheng Huang, and Guang-tao Sun, Ultrahigh cycle fatigue fracture mechanism of high-quality bearing steel obtained through different deoxidation methods, *Int. J. Miner. Metall. Mater.*, 28(2021), No. 5, pp. 804-815. https://doi.org/10.1007/s12613-021-2253-y

---

International Journal of Minerals, Metallurgy and Materials
Volume 28, Number 5, May 2021, Page 804
https://doi.org/10.1007/s12613-021-2253-y

Ultrahigh cycle fatigue fracture mechanism of high-quality bearing steel obtained through different deoxidation methods

Wei Xiao[1)], *Yan-ping Bao*[1)], *Chao Gu*[1)], *Min Wang*[1)], *Yu Liu*[2)], *Yong-sheng Huang*[2)], *and Guang-tao Sun*[2)]

1) State Key Laboratory of Advanced Metallurgy, University of Science and Technology Beijing, Beijing 100083, China
2) ZENITH Steel Group Co. Ltd., Changzhou 213000, China
(Received: 30 July 2020; revised: 14 January 2021; accepted: 18 January 2021)

Abstract: The mechanism of oxide inclusions in fatigue crack initiation in the very-high cycle fatigue (VHCF) regime was clarified by subjecting bearing steels deoxidized by Al (Al-deoxidized steel) and Si (Si-deoxidized steel) to ultrasonic tension–compression fatigue tests (stress ratio, $R = -1$) and analyzing the characteristics of the detected inclusions. Results show that the main types of inclusions in Si- and Al-deoxidized steels are silicate and calcium aluminate, respectively. The content of calcium aluminate inclusions larger than 15 μm in Si-deoxidized steel is lower than that in Al-deoxidized steel, and the difference observed may be attributed to different inclusion generation processes during melting. Despite differences in their cleanliness and total oxygen contents, the Si- and Al-deoxidized steels show similar VHCF lives. The factors causing fatigue failure in these steels reveal distinct differences. Calcium aluminate inclusions are responsible for the cracks in Al-deoxidized steel. By comparison, most fatigue cracks in Si-deoxidized steel are triggered by the inhomogeneity of a steel matrix, which indicates that the damage mechanisms of the steel matrix can be a critical issue for this type of steel. A minor portion of the cracks in Si-deoxidized steel could be attributed to different types of inclusions. The mechanisms of fatigue fracture caused by calcium aluminate and silicate inclusions were further analyzed. Calcium aluminate inclusions first separate from the steel matrix and then trigger crack generation. Silicate inclusions and the steel matrix are closely combined in a fatigue process; thus, these inclusions have mild effects on the fatigue life of bearing steels. Si/Mn deoxidation is an effective method to produce high-quality bearing steel with a long fatigue life and good liquid steel fluidity.

Keywords: bearing steel; non-aluminum deoxidation; inclusion; fatigue crack initiation; tessellated stresses

1. Introduction

Bearing steel is widely used in machinery, automobiles, and other industries, and thus requires high reliability [1]. The growth of the manufacturing industry has steadily improved not only the quality and service time of mechanical equipments but also the quality of the corresponding materials used for mechanical equipments.

Al deoxidation with high-basicity slag is commonly adopted to produce bearing steels in China. The inclusions in Al-deoxidized bearing steels mainly include TiN, MnS, and oxides, the most common of which are spinel ((Mg)–Al–O), calcium aluminate (Ca–Al–O), and silicate (Si–(Al)–O) [2–3]. Calcium aluminate and spinel are deemed the most harmful oxides to the fatigue life (N_f) of bearing steel [4–5]. Gu *et al.* [6] compared the fatigue properties of three types of bearing steels and found that the critical size of spinel inclusions is smaller than that of calcium aluminate.

A general method used to improve the quality of bearing steel is the reduction of the total oxygen (T.O) content to reduce the number of inclusions in Al-deoxidized steel [7–8]. However, calcium aluminate still forms in Al-deoxidized steels, and these inclusions exert great harm to the mechanical characteristics, especially fatigue property, of these steels [9–11]. Unfortunately, efforts to further reduce T.O contents by eliminating calcium aluminate could greatly increase the difficulty of production. The production of high-quality Al-deoxidized bearing steel is further impeded by nozzle clogging and poor control of titanium nitride formation.

Developments in the metallurgical equipment technology, especially the application of Ruhrstahl–Hereaeus (RH) refining to bearing steel smelting [12], have resulted in a new smelting method called non-Al deoxidation to change the main inclusions in the resultant steel into silicate. This method has been widely used in the production of spring steel, saw-wire steel, and cord steel [13–15]. Some scholars have reported trials of the production of bearing steels by this method. Shimamoto *et al.* [16–17] used silicon as a deoxid-

Corresponding author: Yan-ping Bao E-mail: baoyp@ustb.edu.cn

Springer

izer for smelting bearing steel and found that the rated service life (L_{10}) of this steel is greater than 2×10^8 revolutions. Gu *et al.* [18] found that the effect of oxide inclusions generated during Al deoxidation on the N_f is more extensive than that of oxide inclusions produced during Si deoxidation.

In this study, the merits of deoxidation with Si/Mn alloy to produce high-quality bearing steel were assessed. Al-deoxidized steel was produced via the electric arc furnace (EAF)–ladle furnace (LF)–vacuum degassing (VD)–continuous casting (CC) process with Al deoxidation, and Si-deoxidized steel was obtained via the basic oxygen furnace (BOF)–LF–RH–CC process with Si–Mn deoxidation. Differences in the main components, inclusion types, and the effects of these inclusions were compared, and the corresponding fatigue failure mechanisms under high-N_f conditions were studied by ultrahigh cycle fatigue tests. The results of this study provide theoretical guidance for the production of high-quality bearing steel.

2. Experimental

2.1. Fatigue test

The N_f of high-quality bearing steel is greater than 10^7 cycles. Costs may increase if the conventional test method is used. When the N_f of steel reaches 10^9 cycles, the test may take over 116 d to complete, as shown in Fig. 1. Therefore, the ultrasonic fatigue test system was used for the ultrahigh cycle fatigue tests in this study. Because the test frequency of this system is 20 kHz, the test time can be significantly shortened.

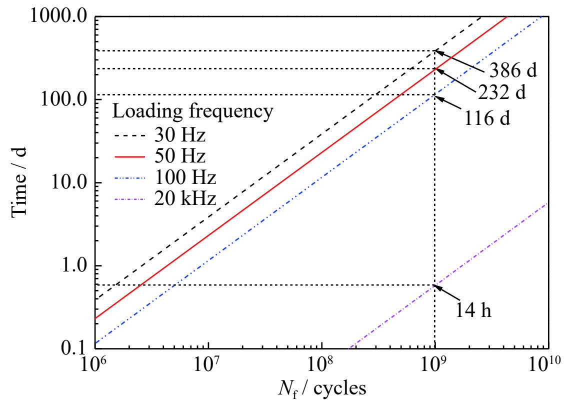

Fig. 1. Relationship between fatigue test time and fatigue cycles.

A schematic of the ultrasonic fatigue test system is shown in Fig. 2. The system can turn electric energy into the mechanical vibration energy of a specific frequency and then output the same via ultrasonic generation, energy conversion, signal acquisition, and cyclic loading control. When a specimen made of different materials is designated according to Xue [19], the natural frequency of this specimen becomes similar to the loading frequency in the loading direction of the system. During the experiment, the specimen is deformed in the resonance mode for fatigue loading.

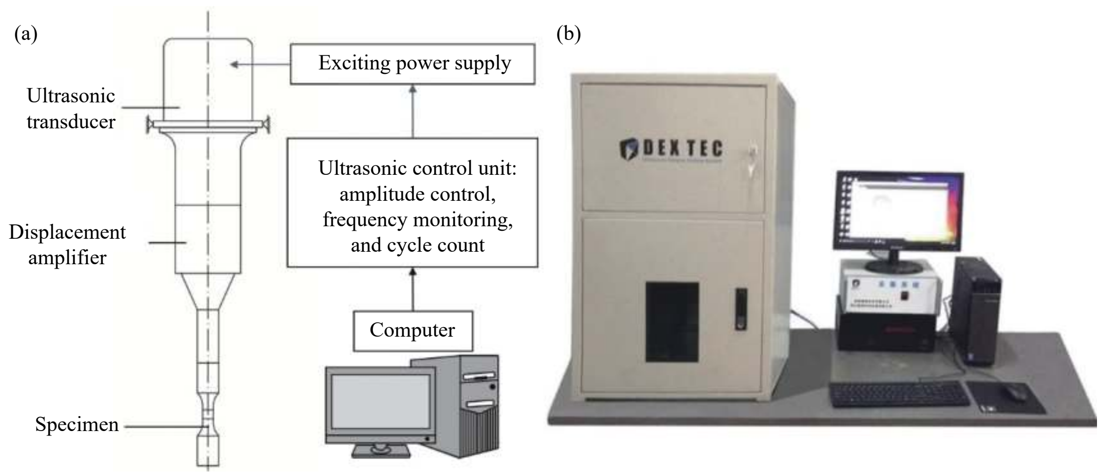

Fig. 2. (a) Schematic [20–22] and (b) physical representation of the ultrasonic fatigue test system.

The fatigue specimens were cut from the edge of rolled bars of bearing steel to maintain the same microstructures and inclusions. The sample position and sketch are shown in Fig. 3. The specimens were treated by spheroid annealing (835°C, 20 min), quenching (oil), and tempering (180°C, 120 min) before the final polishing. The final polishing was performed in the axial direction to reduce the influence of surface defects during the fatigue tests. The fatigue tests were conducted under a resonance frequency of 20 kHz, fully reversible tension–compression (stress ratio, $R = -1$), and air cooling.

The tests were ended when cracks developed on the specimens, and the fracture surfaces were analyzed by scanning electron microscope–energy dispersive spectrometer (SEM–EDS, MLA250, FEI, USA).

2.2. Experimental materials and production processes

Industrial tests of GCr15 bearing steel treated by Al- and

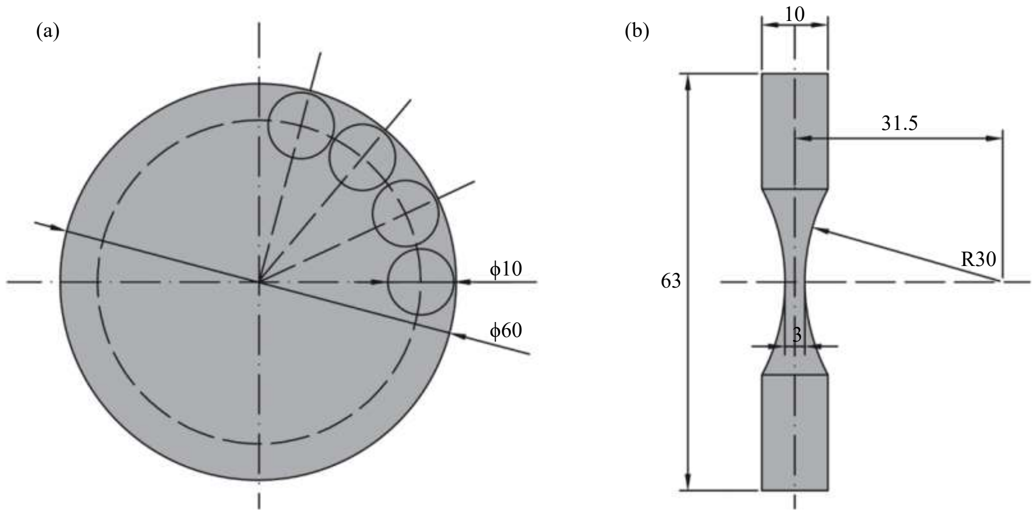

Fig. 3. (a) Sample position and (b) sketch of specimens used for the ultrasonic fatigue test (Unit: mm).

Si-deoxidation were conducted. The main chemical components of the steel samples are shown in Table 1.

The processes of both industrial tests are shown in Fig. 4. Al-deoxidized steel was prepared using an EAF → LF →VD → CC process with Al as the deoxidizer. Si-deoxidized steel was prepared via the BOF → LF → RH → CC process.

Table 1. Main chemical components of the Al- and Si-deoxidized steels

Sample	Type of deoxidation	C / wt%	Si / wt%	Mn / wt%	P / wt%	S / wt%	Cr / wt%	Al / wt%	T.O / ppm
Al-deoxidized steel	Al deoxidation	0.99	0.223	0.338	0.0136	0.0013	1.37	0.009	4
Si-deoxidized steel	Si deoxidation	1.00	0.276	0.332	0.0151	0.0044	1.37	<0.004	10

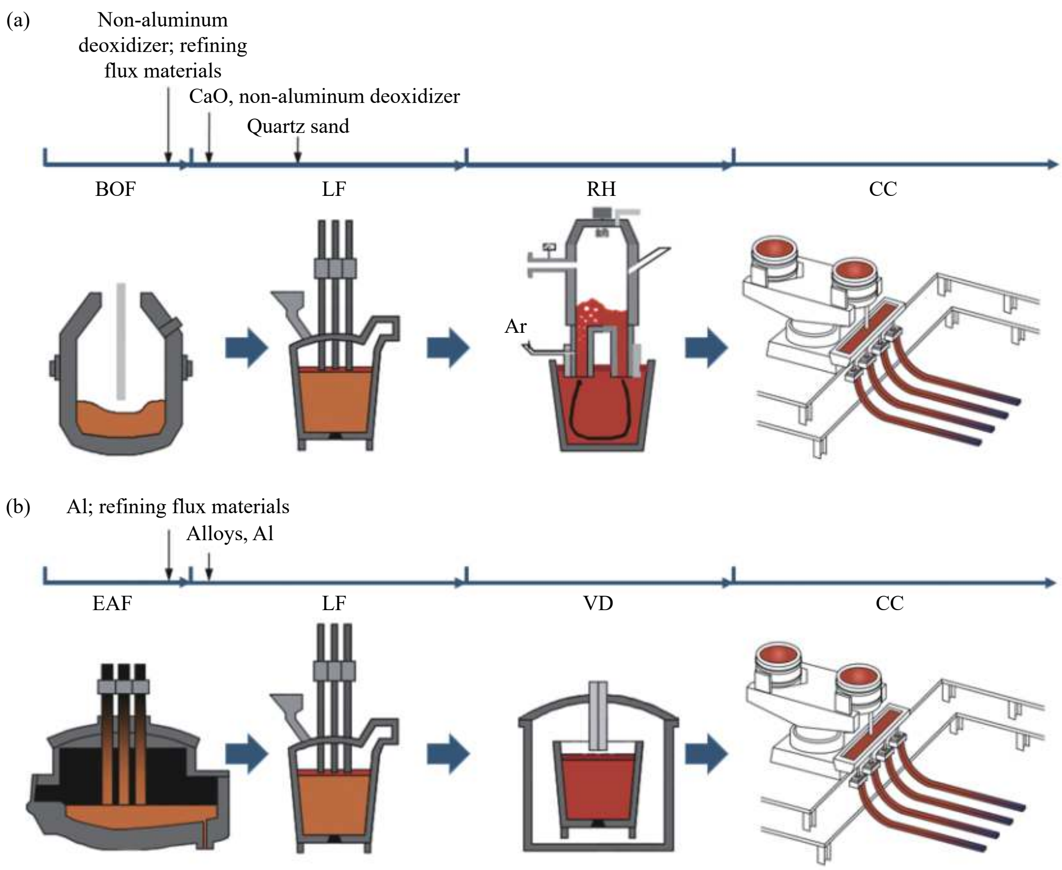

Fig. 4. Industrial processes to obtain (a) Si-deoxidized and (b) Al-deoxidized steels.

Herein, the Si–Mn alloy was added as the deoxidizer to the liquid steel during tapping and LF refining. After CC, the billets were rolled into round bars measuring 60 mm in diameter.

2.3. Inclusion analysis

Steel samples (10 mm × 10 mm × 10 mm) were obtained from the edge of the rolled bars to determine the composition, size, shape, and position of inclusions in the cross section of the bars. The samples were ground and polished using a sandpaper polishing cloth. Inclusions larger than 1 μm in size were detected in the target area (30 mm^2) using an automatic inclusion analysis system (EVO18, Zeiss, Oberkochen, Germany) and then classified according to the compositions determined by the system.

3. Results and discussion

3.1. Characterization of inclusions in steel obtained by different deoxidation methods

Fig. 5 shows the properties of the main inclusions detected in the Al- and Si-deoxidized steels by the automatic inclusion analysis. The composition, size, shape, and more information of inclusions greater than 1 μm in size were detected over a 30-mm^2 area. The classifications in Figs. 5(a) and 5(b) were obtained according to the different elements of the inclusions. In Fig. 5(a), the number of oxide inclusions in Si-deoxidized steel is greater than that in Al-deoxidized steel, consistent with the trend of T.O contents in Si- (10 ppm) and Al-deoxidized steel (4 ppm). However, the numbers and sizes of different oxide inclusions differ between the samples, as observed in Fig. 5(b). The oxide inclusions in Si-deoxidized steel mainly consist of silicate with a number density of 5.19 mm^{-2}. Moreover, the number densities of spinel and calcium aluminate in this sample are less than 0.85 mm^{-2}. By comparison, the number densities of calcium aluminate, spinel, and silicate in Al-deoxidized steel are 1.92, 1.68, and 1.14 mm^{-2}, respectively. Oxide inclusions larger than 15 μm in size, especially calcium aluminate inclusions, are more abundant in Al-deoxidized steel than in Si-deoxidized steel.

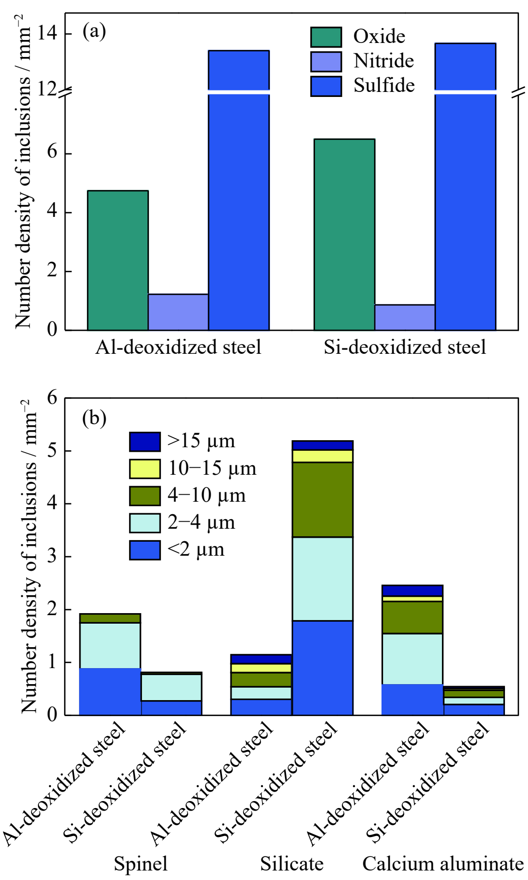

Fig. 5. Comparison of inclusions in Al- and Si-deoxidized steels: (a) number density; (b) size characterization of main oxide inclusions.

Fig. 6 shows the images of typical inclusions in Al- and Si-deoxidized steels determined by SEM-EDS. The morphology of spinel inclusions in Si-deoxidized steel is similar to that in Al-deoxidized steel. However, long inclusions that are mainly composite inclusions wrapped by MnS or containing Si (Table 2) are observed in Si-deoxidized steel but not in Al-deoxidized steel.

3.2. Comparison of inclusion generation mechanism under different deoxidation methods

Calcium aluminate is considered one of the most harmful inclusions for the fatigue property of bearing steels. Thus, the size and number density of this inclusion should be strictly controlled. In this study, the sizes of calcium aluminates in the Al- and Si-deoxidized steels show distinct variations, likely because of the different evolution processes of these inclusions under the two deoxidation methods.

During the melting process, various transient and final oxide inclusions are generated in the molten steel, including alumina (Al_2O_3), spinel ($MgO \cdot Al_2O_3$), calcium aluminates ($CaO \cdot 6Al_2O_3$, $CaO \cdot 2Al_2O_3$, $CaO \cdot Al_2O_3$, and $12CaO \cdot 7Al_2O_3$), and silicates ($SiO_2 \cdot Al_2O_3$). The primary inclusion in the Al-deoxidation process is alumina, whereas the primary inclusion in the non-Al-deoxidation process is silicate.

Aggregation behavior of the initial inclusions greatly affects the size of subsequent inclusions, and this behavior is affected by the capillary force between inclusions [23–24]. According to Yin *et al.* [25–26], the capillary force between solid inclusions is greater than that between liquid inclusions, and liquid inclusions grow much faster when they coalesce with solid inclusions rather than other liquid inclusions. Herein, Factsage7.2 (CRCT-ThermFact Inc., Montreal, Quebec, Canada and GTT-Technologies, Aachen, North Rhine-Westphalia, Germany) was used to calculate the isotherms in the ternary phase diagrams of $CaO–Al_2O_3–SiO_2$ and $CaO–Al_2O_3–MgO$ at 1650°C, as shown in Fig. 7, to clarify the form of transient and final oxide inclusions in the smelt-

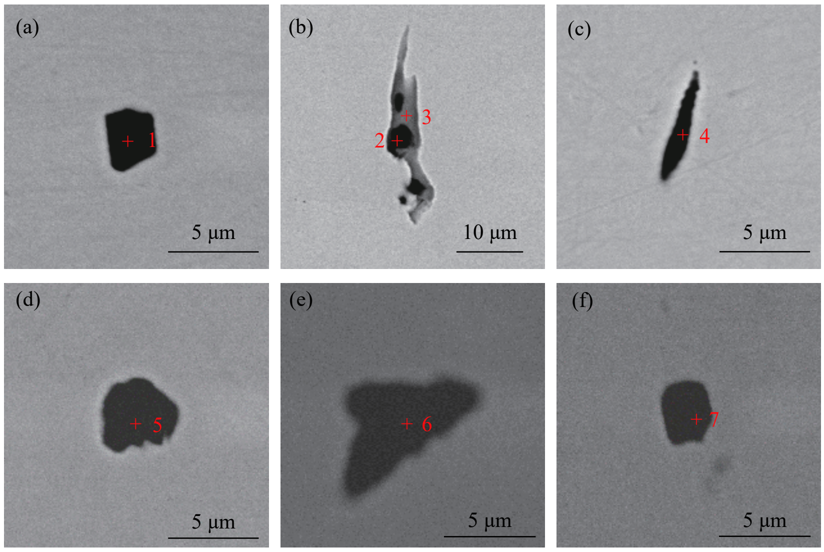

Fig. 6. Typical inclusions in (a)–(c) Si-deoxidized steel and (d)–(e) Al-deoxidized steel.

Table 2. EDS analyses of points 1–7 in Fig. 6 wt%

Point	O	Mg	Al	Si	Ca	Mn	S	Ti
1	34.86	4.49	44.46	—	—	—	—	—
2	21.33	5.14	19.29	—	—	25.12	15.86	2.07
3	—	—	0.67	—	—	41.79	29.42	—
4	19.55	0.85	17.42	8.95	1.07	1.08	—	—
5	34.57	14.68	29.23	—	6.19	—	5.53	—
6	37.58	—	54.15	—	—	—	—	—
7	34.01	16.67	36.93	—	—	—	—	—

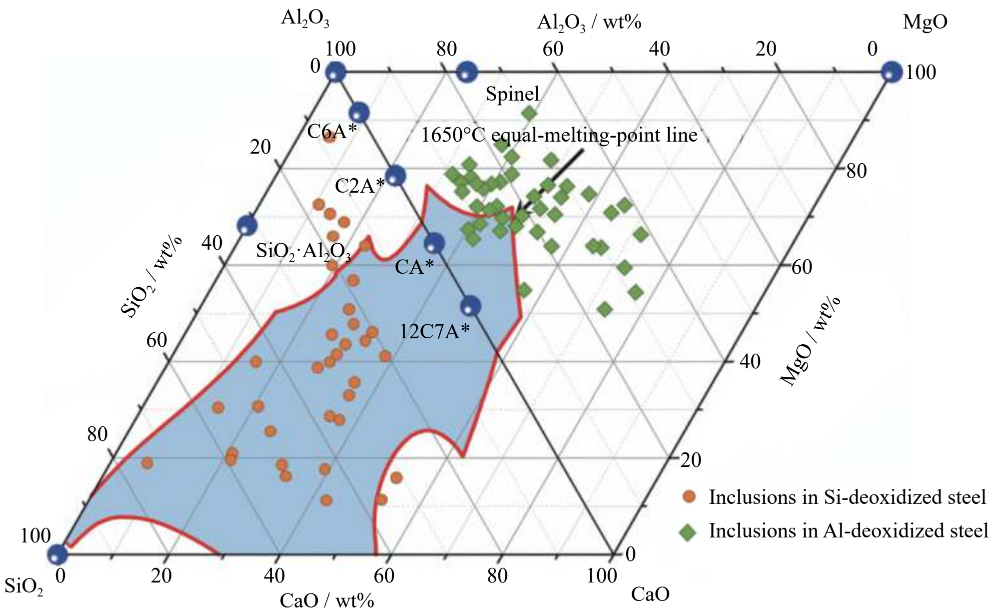

* *m*C*n*A represents calcium aluminum *m*CaO·*n*Al_2O_3

Fig. 7. Ternary phase diagrams of CaO–Al_2O_3–SiO_2 and CaO–Al_2O_3–MgO and the forms of inclusions at 1650°C.

ing process of bearing steel. In the figure, the blue area in the red line is the liquid area at 1650°C. Among all types of inclusions indicated in the figure, only CaO·Al_2O_3 and 12CaO·7Al_2O_3 are liquid at 1650°C.

Xuan *et al.* [27] proposed that the main forces affecting inclusion aggregation in liquid steel are Van der Waals forces and wettability of the inclusions. Van der Waals forces are short-range forces with an action distance ranging from approximately 1–2 μm to the nanometer level. According to Wang [28], the wettability of inclusions is positively related to their Van der Waals forces, i.e., as the wettability between inclusions and liquid steel improves, the Van der Waals forces between inclusions tend to increase. However, the wettability of inclusions shows a negative correlation with the contact angle (θ) between these inclusions and liquid steel, i.e., the smaller the contact angle, the better the wettability of inclusions.

The θ of some inclusions are listed in Table 3 to study the capillary force between solid inclusions of the same size and type.

Table 3. Contact angles (θ) of different types of solid inclusions (°)

Al_2O_3	MgO	$MgO·Al_2O_3$	$CaO·6Al_2O_3$	$CaO·2Al_2O_3$	$SiO_2·Al_2O_3$	SiO_2
142 [29]	134 [30]	125 [31]	126 [30]	120 [31]	130 [29]	113 [29]

According to Table 3, the values of θ that represent the strength of capillary forces between solid inclusions, show the order Al_2O_3 > MgO > $SiO_2·Al_2O_3$ > $CaO·6Al_2O_3$ > $MgO·Al_2O_3$ > $CaO·2Al_2O_3$ > SiO_2. Al_2O_3 inclusions easily gather in liquid steel. Thus, when the primary inclusion is Al_2O_3, the inclusions subsequently generated grow larger than the primary inclusions, although they may be refined by some elements in molten steel such as Mg. However, when the primary inclusion is not Al_2O_3 (e.g., silicate), the sizes of the primary inclusions will be relatively small because they are difficult to aggregate and grow. Thus, the subsequent and final inclusions will also tend to be small. In this study, the complex calcium aluminate inclusions in Al-deoxidized steel originate from alumina, whereas the complex calcium aluminate inclusions in Si-deoxidized steel originate from silicate. Therefore, the sizes of calcium aluminate and silicate in Si-deoxidized steel with silicate as the primary inclusion are relatively smaller than those in Al-deoxidized steel with alumina as the primary inclusion.

The different sizes of these two inclusions may be attributed to differences in their evolution processes under the two deoxidation methods. Kinetic energy-promoting conditions such as gas machine stirring and removal of inclusions by adsorption of refining slag during LF or RH refining are critical to inclusion collision and growth. The effect of RH refining on inclusions was described in a previous study [5]. Other aspects will be described in a future study.

3.3. Characterization of ultrahigh cycle fatigue performance

The ultrahigh cycle fatigue performance of the specimens was evaluated by an ultrasonic fatigue test system. After the cracks occurred in the specimens, the fracture surfaces were observed by SEM–EDS to analyze the origin of crack initiation. In this study, cracks in the specimens were initiated by the steel matrix and inclusions and contained nitride, calcium aluminate, spinel, and silicate. Fig. 8(a) shows the fatigue data with internal crack initiation. The solid points represent broken specimens initiated by inclusions, half-solid points represent broken specimens initiated by the matrix, and “×” represents unbroken specimens. The fatigue performance of Si-deoxidized steel is slightly better than that of Al-deoxidized steel, but their fatigue mechanisms are different, i.e., these two steels show completely different patterns of crack initiation. The number of crack initiations was counted, and the ratio of fatigue crack initiations caused by different inclusions and the steel matrix was calculated as shown in Fig. 8(b). All of the fatigue cracks are initiated by inclusions in Al-deoxidized steel; by contrast, the proportion of fatigue cracks initiated by inclusions in Si-deoxidized steel is only 39%. Interestingly, 61% of the fatigue cracks in Si-deoxidized steel may be attributed to steel matrix inhomogeneity. All the inclusions observed in the fatigue crack initiation sites in Al-deoxidized steel are calcium aluminate; by comparison, nitride, silicate, and spinel but not calcium aluminate are included in Si-deoxidized steel. Although many MnS inclu-

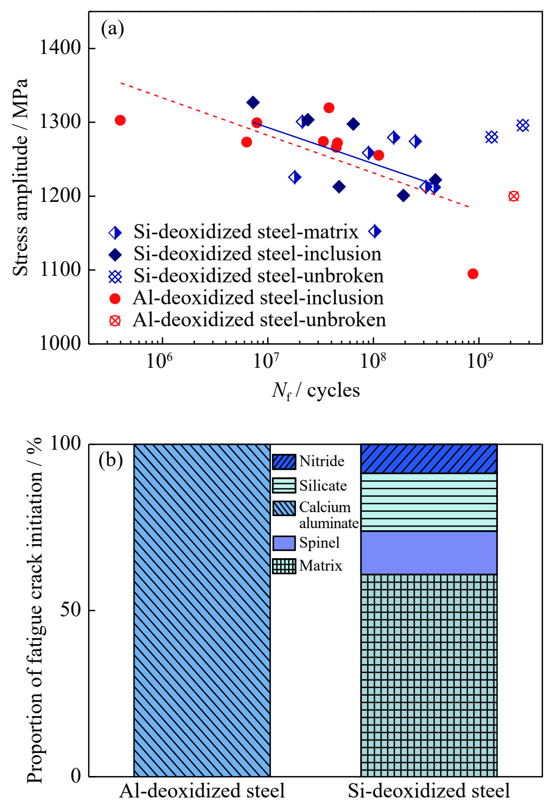

Fig. 8. (a) Stress amplitude–N_f data with internal crack initiation and (b) the ratio of fatigue crack initiation caused by inclusion and steel matrix.

sions exist in Si-deoxidized steel, no fatigue crack initiated by MnS inclusions was found in any of the specimens. Fig. 8(a) reveals that the distribution of data points of cracks caused by inclusions and the matrix is uniform and not related to the stress amplitude in Si-deoxidized steel. This finding indicates a competitive relationship between the inclusions and matrix during the formation of fatigue cracks.

3.4. Relationship between the fatigue cracks caused by inclusions and inclusion characteristics

Murakami and Usuki [32] reported the relationship between the maximum stress intensity factor $K_{\text{max, inc}}$, square root of the area of the internal inclusion $\sqrt{\text{area}}$, and fatigue stress amplitude σ_0. Gu *et al.* [33–34] proposed a 3D analytical equation relating N_f, stress amplitude, and inclusion size in the VHCF regime ($10^7 \le N_f \le 10^9$). According to Murakami and Usuki [32], when $R = -1$, $K_{\text{max, inc}}$ can be expressed using Eq. (1).

$$K_{\text{max, inc}} = 0.5\sigma_0 \sqrt{\pi \sqrt{\text{area}}} \tag{1}$$

The relationship between the growth behavior of fatigue cracks and the size of inclusions during the fatigue loading process is described in Eq. (1). Other parameters of inclusions, such as their types, are not considered in this equation. The influence of different types of inclusions on the fatigue behavior of the steel shows some variations. According to Fig. 8(b), calcium aluminate and silicate inclusions are the most common crack initiators in Al- and Si-deoxidized steels, respectively. The values of $\sqrt{\text{area}}$ and σ_0 for each fracture caused by these two types of inclusions are introduced in Eq. (1), and the relationship between N_f and $K_{\text{max, inc}}$ is obtained to analyze the influence of inclusions on the fatigue behavior of deoxidized steel. Fig. 9 illustrates the relation between $K_{\text{max, inc}}$ and the N_f of steel samples based on the fatigue data according to Gu *et al.* [6] and the present study. The same Al-deoxidation GCr15 bearing steels were used to analyze fatigue properties in both studies. Thus, the $K_{\text{max, inc}}$ of calcium aluminate in both studies can be counted into the same category. In the figure, the type of inclusion clearly influences the value of $K_{\text{max, inc}}$. The $K_{\text{max, inc}}$ values of silicate and calcium aluminate inclusions lie in the same area, whereas the $K_{\text{max, inc}}$ of spinel inclusions lies in low-lying areas. Considering all the $K_{\text{max, inc}}$ presented in Gu's [6] and the present study, the minimum $K_{\text{max, inc}}$ value is 4.00 MPa·m$^{0.5}$ for calcium aluminate inclusions and 3.56 MPa·m$^{0.5}$ for silicate inclusions.

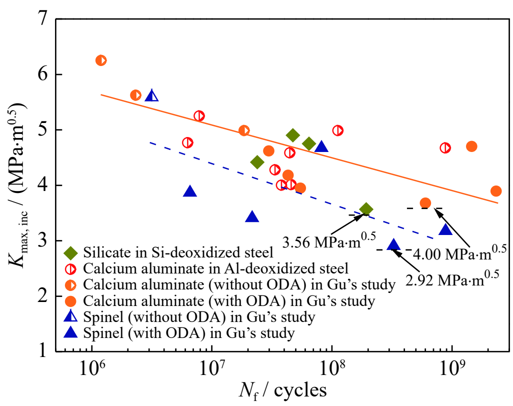

Fig. 9. $K_{\text{max, inc}}$ for the silicate and calcium aluminate inclusions in this study and the spinel and calcium aluminate inclusions in Gu's study [6] (ODA—Optical dark area).

Fig. 10 shows the critical sizes of different inclusions obtained under different fatigue stress amplitudes calculated using Eq. (1) according to the minimum $K_{\text{max, inc}}$. Fatigue cracks are initiated when the size of an inclusion is larger than its critical size. In the figure, the critical sizes of silicate and calcium aluminate inclusions decrease with increasing stress amplitude. Under the same stress amplitude, the critical size of silicate inclusions is smaller than that of calcium aluminate inclusions. For example, when the stress amplitude is 1200 MPa, the critical size of silicate inclusions is 12.68 μm, whereas that of calcium aluminate inclusions is 15.97 μm. Thus, the ratio of inclusion sizes larger than the corresponding critical size was calculated according to the characterization of inclusions shown in Fig. 5. The results show that the ratio of sizes larger than the critical size of silicate inclusions is 5.1%; by comparison, the ratio of sizes larger than the critical size of calcium aluminate inclusions is 8.2%. These findings may explain why the fatigue performance of Si-deoxidized steel is better than that of Al-deoxidized steel.

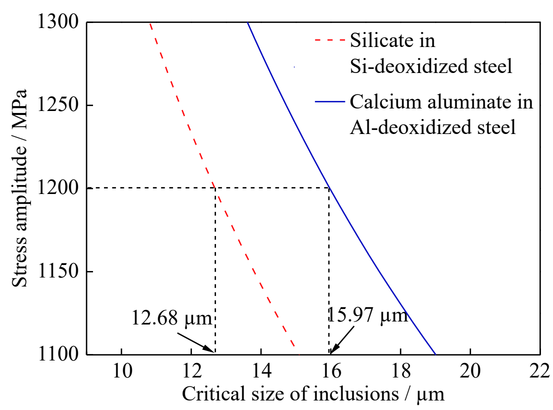

Fig. 10. Critical sizes of silicate inclusions in Si-deoxidized steel and calcium aluminate inclusions in Al-deoxidized steel under different fatigue stress amplitudes.

3.5. Mechanisms of fatigue fracture caused by different inclusions

Because inclusions observed in fatigue crack initiation sites in the Al- and Si-deoxidized steels show great differences, but the steel matrix of both steels are expected to be identical because standard rolling and heat treatment procedures were established, the effects of different inclusions in these two steels must be different. Fig. 11 shows the typical morphologies of fatigue crack fractures and compositions of

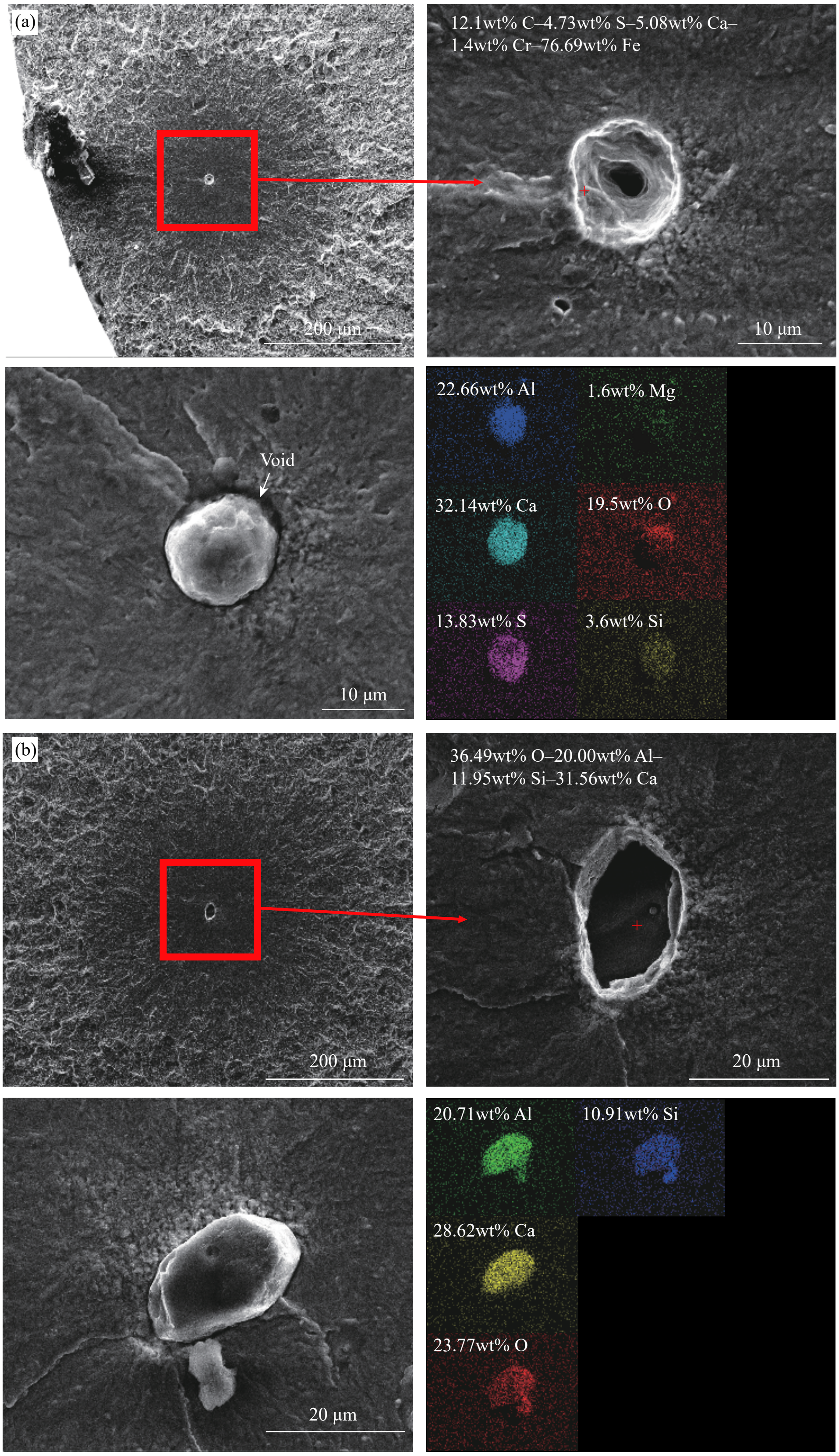

Fig. 11. Typical crack initiation caused by (a) calcium aluminate (σ_0 = 1272 MPa; N_f = 4.57 × 10^7 cycles) and (b) silicate (σ_0 = 1298 MPa; N_f = 6.44 × 10^7 cycles).

inclusions in the crack initiation sites.

Fig. 11 (a) illustrates that calcium aluminate exists as an integral inclusion on one side of the fracture surface and triggers fatigue cracks. Under this case, obvious voids can be observed between the calcium aluminate inclusions and steel matrix. By contrast, Fig. 11(b) shows that silicate inclusions are torn apart and remain on both sides of the broken specimen when fatigue cracks are triggered. Moreover, no void can be observed between the silicate inclusions and steel matrix.

The tessellated stresses between different inclusions and the steel matrix were calculated according to the model of Brooksbank and Andrews [35], expressed in Eqs. (2)–(3), to further understand the mechanisms of void generation. In this model, an inclusion is assumed to be spherical, and the radius of the matrix is greater than that of the inclusion.

$$\sigma_R = \frac{(\alpha_M - \alpha)\Delta T}{\frac{0.5(1+\upsilon_M)+(1-2\upsilon_M)d^3}{E_M(1-d^3)} + \frac{1-2\upsilon}{E}} \quad (2)$$

$$d = R_{in}/R_M \quad (3)$$

where σ_R is the radial stress beneath the inclusion; υ and E are Poisson's ratio and Young's modulus, respectively; subscript M represents the matrix; no subscript represents inclusions; ΔT is the difference in room temperature and the holding temperature before vacuum quenching; and R_{in} is the radius of the inclusion. In this study, inclusions larger than 1 μm in size were detected in the target area (30 mm^2) using an automatic inclusion analysis system. The composition, size, shape, and some other information of these inclusions can be obtained using the system that can also classify the inclusions according to their composition. The density of each type of inclusion, N, can be obtained. Thus, R_{in} is determined from the data, as shown in Fig. 5. R_M is the radius of the steel matrix around one inclusion, which can be calculated from the number density of inclusions as follows: $R_M = 1000\sqrt{\frac{1}{\pi N}}$; herein, α_M and α are the coefficients of linear expansion of the steel matrix and inclusion, respectively. The coefficient of linear expansion of the silicate inclusions is calculated using Eq. (4) [36]:

$$\alpha = \Sigma w_i \alpha_i \quad (4)$$

where w_i is the mass fraction of oxide i in the silicate and is calculated using the average value of all silicates in Si-deoxidized steel, and α_i is the fraction of the coefficient of linear expansion of oxide i in the silicates, as shown in Table 4.

The calculated coefficient of linear expansion of silicate inclusions and other mechanical parameters and coefficients of thermal expansion are shown in Table 5.

The σ_R at the interface between the main inclusions (i.e., calcium aluminate in Al-deoxidized steel and silicate in Si-deoxidized steel) and the steel matrix was calculated based on Eqs. (3)–(4) and parameters in Tables 4 and 5. The yield strength of the steel matrix determined via tensile tests is 1602 MPa. The radius of inclusion (R_{in}) in the calculation refers to the measured maximum size of inclusions in both steels, as shown in Fig. 5. The calculated tessellated stresses of silicate and calcium aluminate are shown in Fig. 12. The tessellated stresses of the yield strength of the steel matrix and different types of inclusions follow the order: calcium aluminate > matrix > silicate.

Table 4. Fractions of the coefficients of linear expansion of oxides

Oxide	Average mass fraction of oxide i, w_i / %	Fraction of the coefficient of linear expansion, α_i / (10^{-7}°C^{-1})
SiO_2	48.2	5–38
CaO	19.5	130
Al_2O_3	29.7	−40
MgO	2.6	60

Table 5. Mechanical parameters and coefficients of thermal expansion [35,37–38]

Material	Coefficient of linear expansion, α / (10^{-6}°C^{-1})	Young's modulus, E / GPa	Poisson's ratio, υ
Silicate	2.47	71	0.21
Calcium aluminate	5.0	113	0.23
Matrix	23.0	206	0.50

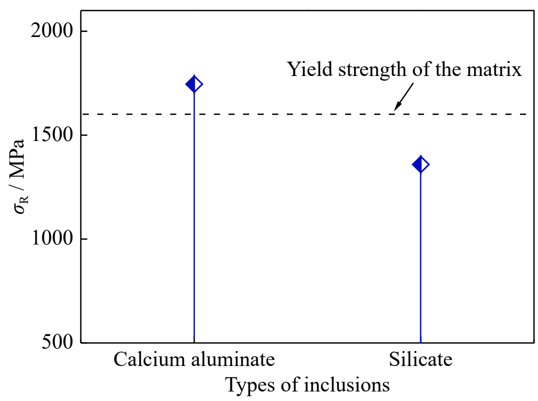

Fig. 12. Effect of inclusion types on tessellated stress.

According to Deng and Zhu [39] and Ma *et al.* [40], plastic deformation in the matrix will occur around inclusions when the yield strength of the steel matrix is smaller than the tessellated stresses of the inclusions and generate voids around these inclusions; no plastic deformation occurs when the yield strength of the steel matrix is larger than the tessellated stresses of the inclusions, which retains a tight bonding between the steel matrix and inclusions. This mechanism is consistent with the morphologies shown in Fig. 11.

The mechanisms of fatigue failure triggered by calcium aluminate and silicate inclusions are summarized in Fig. 13. Herein, the relative yield strength of the inclusions and steel matrix is considered the major factor influencing fatigue failure. However, the bonding strength between the inclusions and matrix, fracture strength of the inclusions, and residual stresses between the inclusions and matrix from the prior manufacturing or heat treatment processes may also be important factors [41]. Fig. 13 illustrates that debonding between calcium aluminate inclusions surrounded by voids and one side of the steel matrix first occurs in Al-deoxidized steel. Fatigue cracks are then initiated in the steel matrix around voids with unbroken inclusions. In Si-deoxidized steel, silicate inclusions break during the fatigue process and remain in both parts of the failure specimen. The different fatigue mechanisms of these two types of inclusions could be attributed to the differences in the mechanical properties of the inclusions and bonding relationships between these inclusions and the steel matrix. In the case of silicate in Si-deoxidized steel, the inclusions and steel matrix are bonded tightly, which generates opposing stresses to the steel matrix compared with tension–compression fatigue loading and reduces the strain of the steel matrix; these phenomena delay the generation of cracks in the steel matrix during tension [42]. In the case of calcium aluminate, debonding between the inclusions and steel matrix, with the generation of voids, eliminates opposing stresses. Therefore, cracks are easily generated in the steel matrix.

Because voids in steels can easily trigger fatigue cracks, the different void features around inclusions, besides the properties of these inclusions, should be taken into account when the effects of inclusions on fatigue behaviors are considered.

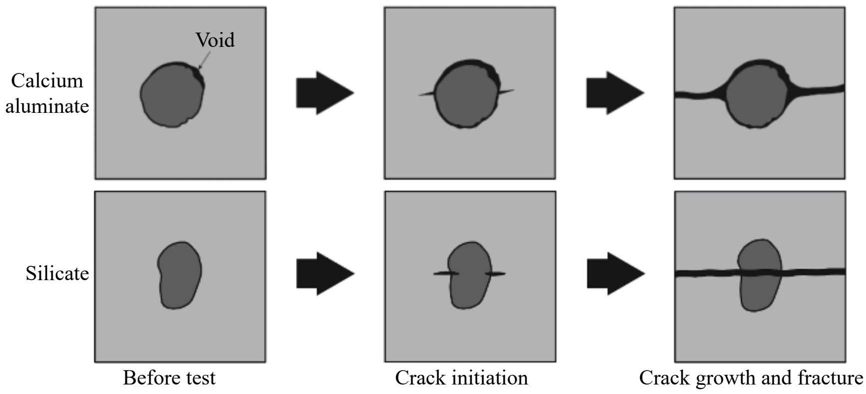

Fig. 13. Mechanism of fatigue fractures caused by different oxide inclusions.

4. Conclusions

In this study, industrial-scale production tests of bearing steels with Al and non-Al deoxidation were conducted. The inclusions in the two types of steels obtained were characterized, and ultrasonic fatigue tests were adopted to clarify the VHCF properties of the steels in terms of different inclusions. The following conclusions were obtained.

(1) The inclusion types of the two steels similarly include spinel, silicate, and calcium aluminate but with different proportions and size features. The main type of inclusion in Si-deoxidized steel is silicate, whereas the main type of inclusion in Al-deoxidized steel is calcium aluminate. The content of calcium aluminate inclusions larger than 15 μm in size in Si-deoxidized steel is obviously lower than that in Al-deoxidized steel. This difference is attributed to differences in the generation processes of this inclusion during melting.

(2) Despite differences in their cleanliness and T.O content, the VHCF lives of Si-deoxidized steel and Al-deoxidized steel are similar; however, the factors causing fatigue failure in these steels showed distinct differences. Calcium aluminate inclusions are responsible for the cracks in Al-deoxidized steel. By comparison, 61% of the fatigue cracks in Si-deoxidized steel is triggered by the inhomogeneity of the steel matrix, and only 39% of the cracks could be attributed to different types of inclusions. When the stress amplitude is 1200 MPa, the critical size of silicate inclusions is 12.68 μm. Under the same stress amplitude, the critical size of calcium aluminate inclusions is 15.97 μm.

(3) Calcium aluminate and silicate inclusions cause different mechanisms of fatigue failure in Al- and Si-deoxidized steels. Calcium aluminate inclusions first separate from the steel matrix side and then generate cracks. Silicate inclusions and the steel matrix are closely combined in the fatigue process; thus, these inclusions have mild effects on the fatigue life of bearing steels. However, as the damage mechanisms of the steel matrix may be a critical issue for Si-deoxidized steel, further research on these mechanisms is necessary.

(4) The ultrahigh cycle fatigue life of bearing steel deoxidized by Si/Mn with a T.O content of 10 ppm is similar to that of bearing steel deoxidized by Al with T.O content of 4 ppm. Inclusion detection and ultrahigh cycle fatigue failure mechanism analysis confirm that Si/Mn-deoxidized bearing steel can have higher T.O contents than Al-deoxidized bearing steel but maintain a longer ultrahigh cycle fatigue life. Therefore, Si/Mn-deoxidation is an effective method to produce

high-quality bearing steel with a long fatigue life and good liquid steel fluidity.

Acknowledgements

This work was financially supported by the National Natural Science Foundation of China (No. 51774031), the Fundamental Research Funds for the Central Universities (No. FRF-TP-20-026A1), and the State Key Laboratory of Advanced Metallurgy Foundation (No. 41620001).

References

[1] S.M. Wang, Q. Lü, H.L. Wang, and M. Liang, Behavior of nonmetallic inclusions in casting slab of BOF bearing steel, *J. Northeast. Univ.*, 27(2006), No. 2, p. 192.

[2] L. Yang and G.G. Cheng, Characteristics of Al_2O_3, MnS, and TiN inclusions in the remelting process of bearing steel, *Int. J. Miner. Metall. Mater.*, 24(2017), No. 8, p. 869.

[3] M. Luo and J.G. Wang, Effects of nonmetallic inclusions on initiation and propagation of rolling contact fatigue cracks, *Bearing*, 2020, No. 6, p. 58.

[4] M. Li, X.C. Wang, J.H. Duan, W. Yang, G. Cheng, L. Wang, L.W. Yang, and L.F. Zhang, Formation and controlling of type-D inclusions in bearing steel, *Chin. J. Eng.*, 40(2018), Suppl. 1, p. 31.

[5] W. Xiao, M. Wang, and Y.P. Bao, The research of low-oxygen control and oxygen behavior during RH process in silicon-deoxidization bearing steel, *Metals*, 9(2019), No. 8, art. No. 812.

[6] C. Gu, M. Wang, Y.P. Bao, F.M. Wang, and J.H. Lian, Quantitative analysis of inclusion engineering on the fatigue property improvement of bearing steel, *Metals*, 9(2019), No. 4, art. No. 476.

[7] T. Kamiya, K. Mizobe, and K. Kida, Effect of observation position of SUJ2 bar specimens on inclusions distribution, *IOP Conf. Ser.: Mater. Sci. Eng.*, 307(2018), art. No. 12046.

[8] C. Gu, Y.P. Bao, P. Gan, M. Wang, and J.S. He, Effect of main inclusions on crack initiation in bearing steel in the very high cycle fatigue regime, *Int. J. Miner. Metall. Mater.*, 25(2018), No. 6, p. 623.

[9] S.M. Moghaddam and F. Sadeghi, A review of microstructural alterations around nonmetallic inclusions in bearing steel during rolling contact fatigue, *Tribol. Trans.*, 59(2016), No. 6, p. 1142.

[10] K. Hashimoto, T. Fujimatsu, N. Tsunekage, K. Hiraoka, K. Kida, and E.C. Santos, Effect of inclusion/matrix interface cavities on internal-fracture-type rolling contact fatigue life, *Mater. Des.*, 32(2011), No. 10, p. 4980.

[11] Y. Neishi, T. Makino, N. Matsui, H. Matsumoto, M. Higashida, and H. Ambai, Influence of the inclusion shape on the rolling contact fatigue life of carburized steels, *Metall. Mater. Trans. A*, 44(2013), No. 5, p. 2131.

[12] J.L. Guo, L.H. Zhao, Y.P. Bao, S. Gao, and M. Wang, Carbon and oxygen behavior in the RH degasser with carbon powder addition, *Int. J. Miner. Metall. Mater.*, 26(2019), No. 6, p. 681.

[13] X.F. Cai, Y.P. Bao, L. Lin, and C. Gu, Effect of Al content on the evolution of non-metallic inclusions in Si–Mn deoxidized steel, *Steel Res. Int.*, 87(2016), No. 9, p. 1168.

[14] S.H. Chen, M. Jiang, X.F. He, and X.H. Wang, Top slag refining for inclusion composition transform control in tire cord steel, *Int. J. Miner. Metall. Mater.*, 19(2012), No. 6, p. 490.

[15] Y. Li, C.Y. Chen, G.Q. Qin, Z.H. Jiang, M. Sun, and K. Chen, Influence of crucible material on inclusions in 95Cr saw-wire steel deoxidized by Si–Mn, *Int. J. Miner. Metall. Mater.*, 27(2020), No. 8, p. 1083.

[16] M. Shimamoto, E. Tamura, A. Owaki, and A. Matsugasako, Influence of modified oxide inclusions on initiation of rolling contact fatigue cracks in bearing steel, *Kobe Steel Eng. Rep.*, 69(2019), No. 2, p. 90.

[17] M. Shimamoto, T. Sugimura, S. Kimura, A. Owaki, M. Kaizuka, and Y. Shindo, Improvement of the rolling contact fatigue resistance in bearing steels by adjusting the composition of oxide inclusions, [in] J.M. Beswick, ed., *Bearing Steel Technologies: 10th Volume, Advances in Steel Technologies for Rolling Bearings*, STP1580, ASTM International, West Conshohocken, PA, 2015, p. 173.

[18] C. Gu, Y.P. Bao, P. Gan, J.H. Lian, and S. Münstermann, An experimental study on the impact of deoxidation methods on the fatigue properties of bearing steels, *Steel Res. Int.*, 89(2018), No. 9, art. No. 1800129.

[19] H.Q. Xue, *Investigation on Fatigue Behavior of Materials in Very High Cycle Regime under Vibratory Loading* [Dissertation], Northwestern Polytechnical University, Xi'an, 2006.

[20] T. Wu, J. Ni, and C. Bathias, An automatic ultrasonic fatigue testing system for studying low crack growth at room and high temperatures, [in] C. Amzallag, ed., *Automation in Fatigue and Fracture: Testing and Analysis*, STP1231, ASTM International, West Conshohocken, PA, 1994, p. 598.

[21] L.D. Roth, Ultrasonic fatigue testing, [in] H. Kuhn and D. Medlin, eds., *Mechanical Testing and Evaluation*, ASM Handbook, Vol. 8, ASM International, Materials Park, OH, 2000, p. 1659.

[22] W.P. Mason and H. Baerwald, Piezoelectric crystals and their applications to ultrasonics, *Phys. Today*, 4(1951), No. 5, p. 23.

[23] S. Kimura, Y. Nabeshima, K. Nakajima, and S. Mizoguchi, Behavior of nonmetallic inclusions in front of the solid–liquid interface in low-carbon steels, *Metall. Mater. Trans. B*, 31(2000), No. 5, p. 1013.

[24] S. Kimura, K. Nakajima, and S. Mizoguchi, Behavior of alumina–magnesia complex inclusions and magnesia inclusions on the surface of molten low-carbon steels, *Metall. Mater. Trans. B*, 32(2001), No. 1, p. 79.

[25] H.B. Yin, H. Shibata, T. Emi, and M. Suzuki, Characteristics of agglomeration of various inclusion particles on molten steel surface, *ISIJ Int.*, 37(1997), No. 10, p. 946.

[26] H.B. Yin, H. Shibata, T. Emi, and M. Suzuki, "*In-situ*" observation of collision, agglomeration and cluster formation of alumina inclusion particles on steel melts, *ISIJ Int.*, 37(1997), No. 10, p. 936.

[27] C.J. Xuan, A.V. Karasev, P.G. Jönsson, and K. Nakajima, Attraction force estimations of Al_2O_3 particle agglomerations in the melt, *Steel Res. Int.*, 88(2017), No. 2, art. No. 1600090.

[28] L.Z. Wang, *Study on the Refinement and Homogenized Distribution of Inclusions in Al Killed Steel* [Dissertation], University of Science and Technology Beijing, Beijing, 2017.

[29] K. Raiber, P. Hammerschmid, and D. Janke, Experimental studies on Al_2O_3 inclusion removal from steel melts using ceramic filters, *ISIJ Int.*, 35(1995), No. 4, p. 380.

[30] K. Nogi and K. Ogino, Role of interfacial phenomena in deoxidation process of molten iron, *Can. Metall. Q.*, 22(1983), No. 1, p. 19.

[31] N. Shinozaki, N. Echida, K. Mukai, Y. Takahashi, and Y. Tanaka, Wettability of Al_2O_3–MgO, ZrO_2–CaO, Al_2O_3–CaO sub-

strates with molten iron, *Tetsu-to-Hagané*, 80(1994), No. 10, p. 748.

[32] Y. Murakami and H. Usuki, Quantitative evaluation of effects of non-metallic inclusions on fatigue strength of high strength steels. II: Fatigue limit evaluation based on statistics for extreme values of inclusion size, *Int. J. Fatigue*, 11(1989), No. 5, p. 299.

[33] C. Gu, J.H. Lian, Y.P. Bao, Q.G. Xie, and S. Münstermann, Microstructure-based fatigue modelling with residual stresses: Prediction of the fatigue life for various inclusion sizes, *Int. J. Fatigue*, 129(2019), art. No. 105158.

[34] C. Gu, J.H. Lian, Y.P. Bao, and S. Münstermann, Microstructure-based fatigue modelling with residual stresses: Prediction of the microcrack initiation around inclusions, *Mater. Sci. Eng. A*, 751(2019), p. 133.

[35] D. Brooksbank and K.W. Andrews, Tessellated stresses associated with some inclusions in steel, *J. Iron Steel Inst.*, 207(1969), p. 474.

[36] Y. Wang, The relationship between thermal expansion coefficient and chemical composition of glass, *Bull. Chin. Ceram. Soc.*, 1(1982), No. 3, p. 35.

[37] D. Brooksbank and K.W. Andrews, Thermal expansion of some inclusions found in steels and relation to tessellated stresses, *J. Iron Steel Inst.*, 206(1969), p. 595.

[38] K. Yang, B. Yang, X.Y. Xu, C. Hoover, M.M. Smedskjaer, and M. Bauchy, Prediction of the Young's modulus of silicate glasses by topological constraint theory, *J. Non-Cryst. Solids*, 514(2019), p. 15.

[39] Z.Y. Deng and M.Y. Zhu, Evolution mechanism of non-metallic inclusions in Al-killed alloyed steel during secondary refining process, *ISIJ Int.*, 53(2013), No. 3, p. 450.

[40] Y. Ma, T. Pan, B. Jiang, Y.H. Cui, S. Hang, and Y. Peng, Study of the effect of sulfur contents on fracture toughness of railway wheel steels for high speed train, *Acta Metall. Sin.*, 47(2011), No. 8, p. 978.

[41] C. Gu, J.H. Lian, Y.P. Bao, W. Xiao, and S. Münstermann, Numerical study of the effect of inclusions on the residual stress distribution in high-strength martensitic steels during cooling, *Appl. Sci.*, 9(2019), No. 3, art. No. 455.

[42] C. Gu, W.Q. Liu, J.H. Lian, and Y.P. Bao, In-depth analysis of the fatigue mechanism induced by inclusions for high-strength bearing steels, *Int. J. Miner. Metall. Mater.*, 28(2021), 5, p. 826.